The Population Balance Model for Gas−Liquid Flows—Influence of Bubble Coalescence and Breakup Models

ARTICLE *in* INDUSTRIAL & ENGINEERING CHEMISTRY RESEARCH · AUGUST 2005

Impact Factor: 2.59 · DOI: 10.1021/ie0489002

3 AUTHORS, INCLUDING:

Tiefeng Wang
Tsinghua University
84 PUBLICATIONS **875** CITATIONS
SEE PROFILE

Yong Jin
Changshu Institute of Technology
189 PUBLICATIONS **3,119** CITATIONS
SEE PROFILE

Population Balance Model for Gas−Liquid Flows: Influence of Bubble Coalescence and Breakup Models

Tiefeng Wang, Jinfu Wang,* and Yong Jin

Department of Chemical Engineering, Tsinghua University, Beijing 100084, People's Republic of China

In dispersed gas−liquid flows, the bubble size distribution plays an important role in the phase structure and the interphase forces, which, in turn, determine the multiphase hydrodynamic behaviors, including the spatial profiles of the gas fraction, gas and liquid velocities, and mixing and mass-transfer behaviors. The population balance model (PBM) is an effective method to simulate the bubble size distribution. The bubble coalescence and breakup models have a distinct influence on the prediction ability of the PBM. This work compares several typical bubble coalescence and breakup models. The results show that the bubble size distributions predicted by the PBM are quite different when different bubble coalescence and breakup models are used. By using proper bubble coalescence and breakup models, the bubble size distribution and regime transition can be reasonably predicted. The results also show that it is necessary to take into account bubble coalescence and breakup due to different mechanisms.

1. Introduction

In dispersed gas−liquid flows, the bubble size distribution plays an important role in the phase structure and interphase forces, which, in turn, determine the multiphase hydrodynamic behaviors, including the spatial profiles of the gas fraction, gas and liquid velocities, and mixing and mass-transfer behaviors. It is therefore necessary to take into account these influences to get good predictions in wide conditions by the computational fluid dynamics (CFD) simulation. The population balance model (PBM) is an effective method to simulate the bubble size distribution. The PBM was first formulated for chemical engineering purposes by Hulburt and Katz[1] and has drawn much attention from both academic and industrial researches because it can describe the size distribution of the dispersed phase in a wide variety of particulate processes.[2] In recent years, much work has been done using the PBM to simulate the bubble size distribution in gas−liquid flows, which shows the great potential of the PBM in such systems.[3−7]

In the PBM, the bubble coalescence and breakup models are very important for reasonable predictions of the bubble size distribution. Many bubble coalescence and breakup models have been proposed.[8−17] However, some obvious discrepancies exist in these models; for example, the daughter bubble size distributions are greatly different for different bubble breakup models, as reviewed in our previous publication.[18] Therefore, it is necessary to compare the typical bubble coalescence and breakup models that have been commonly used in the literature. This comparison is also valuable for further coupling of the PBM into a CFD framework to get a better understanding of the hydrodynamic behaviors in a gas−liquid flow. This work aims to make a comparison of several typical bubble coalescence and breakup models and to discuss in detail the ability of the PBM to predict the bubble size distribution.

* To whom correspondence should be addressed. Fax: 86-10-62772051. E-mail: wangjf@flotu.org.

2. Population Balance Model

The PBM is a statistical formulation to describe the size distribution of the dispersed phase in a multiphase flow. Generally speaking, the PBM equation for a gas−liquid flow can be expressed as follows:[19]

$$\frac{\partial n(v,t)}{\partial t} + \nabla\cdot[\mathbf{u}_b n(v,t)] = \frac{1}{2}\int_0^v n(v-v',t)\, n(v',t)\, c(v-v',v')\, \mathrm{d}v' - \int_0^\infty n(v,t)\, n(v',t) \times c(v,v')\, \mathrm{d}v' + \int_v^\infty \beta(v,v')\, b(v')\, n(v',t)\, \mathrm{d}v' - b(v)\, n(v,t) \quad (1)$$

Equation 1 is an integrodifferential equation and can only be solved numerically. Different approaches have been proposed in the literature to solve the PBM equation, as reviewed by Ramkrishna.[19] The discretization method developed by Kumar and Ramkrishna[20] was used in this work. In this method, the bubble size is divided into different size subregions, and eq 1 is integrated over each discrete bubble size region. The bubbles with volume unequal to any pivot are redistributed to the two nearest pivots using an approach ensuring the conservation of bubble mass and number. The final discrete PBM is in terms of N_i and reads

$$\frac{\mathrm{d}N_i(t)}{\mathrm{d}t} + \nabla\cdot[\mathbf{u}_b N_i(t)] = \sum_{\substack{j,k \\ g_{i-1}\le g_j+g_k\le g_{i+1}}}^{j\ge k} \left(1-\frac{1}{2}\delta_{j,k}\right)\eta_{i,j,k} c_{j,k} N_j(t)\, N_k(t) - N_i(t)\sum_{k=1}^{M} c_{i,j} N_k(t) + \sum_{k=i}^{M} \zeta_{i,k} b_k N_k(t) - b_i N_i(t) \quad (2)$$

where $c_{j,k} = c(v_i,v_j)$, $b_i = b(v_i)$, M is the number of size subregions, and $\zeta_{i,k}$ and $\eta_{i,j,k}$ are as follows:

$$\zeta_{i,k} = \int_{g_i}^{g_{i+1}} \frac{g_{i+1}-v}{g_{i+1}-g_i}\beta(v,g_k)\, \mathrm{d}v + \int_{g_{i-1}}^{g_i} \frac{v-g_{i-1}}{g_i-g_{i-1}}\beta(v,g_k)\, \mathrm{d}v \quad (3)$$

10.1021/ie0489002 CCC: $30.25
Published on Web 08/13/2005

$$\eta_{i,j,k}=\begin{cases}(g_{i+1}-v)/(g_{i+1}-g_i), & g_i<v\le g_{i+1}\\ (v-g_{i-1})/(g_i-g_{i-1}), & g_{i-1}<v\le g_i\end{cases} \qquad v=v_j+v_k \quad (4)$$

To solve eq 2, the bubble coalescence rate $c(v_i,v_j)$, bubble breakup rate $b(v)$, and daughter bubble size distribution $\beta(v_1,v)$ are needed.

3. Bubble Coalescence and Breakup

The coalescence rate of bubbles of size d_i and d_j can be expressed by

$$c(d_i,d_j) = \varpi_c(d_i,d_j)\, P_c(d_i,d_j) \quad (5)$$

where ϖ_c and P_c are the collision frequency and coalescence efficiency, respectively. Bubble collisions due to turbulent eddies were calculated by analogy with the gas kinetic theory.[9,17] Up to now, models for the bubble coalescence efficiency are mainly based on a phenomenological analysis. According to the bubble coalescence theory, coalescence will occur during a collision of two bubbles provided that the contact time exceeds the coalescence time required for drainage of the liquid film between them to a critical rupture thickness.[21] The ratio between the contact time τ and the coalescence time t can thus provide a first indication of whether coalescence will occur. The following function was used by Lee et al.,[8] Prince and Blanch,[9] and Chesters:[21]

$$P_c(d_i,d_j) = \exp(-t_{ij}/\tau_{ij}) \quad (6)$$

Besides coalescence due to turbulent eddies, bubbles may coalesce as a result of other mechanisms. Prince and Blanch[9] also considered bubble coalescence due to different rise velocities and laminar shear. Fu and Ishii[22] considered bubble coalescence due to wake entrainment. Lehr et al.[17] combined the bubble coalescence due to turbulent eddies and different rise velocities.

The bubble breakup model generally falls into two categories: one is based on the bubble−eddy collision mechanism,[9,14,17,18] and the other is based on kinematic ideas.[11,15] The models based on a bubble−eddy collision mechanism have a clear physical picture and solid theoretical foundation of turbulence and statistics. Therefore, this work focuses on such bubble breakup models.

Four typical bubble coalescence and breakup models were compared. They are the models of Prince and Blanch,[9] Luo and Svendsen,[13,14] Lehr et al.,[17] and Wang et al.[18,23] These models were chosen also with the consideration that these authors gave the bubble coalescence and breakup models simultaneously.

3.1. Models of Prince and Blanch. 3.1.1. Bubble Coalescence. Prince and Blanch[9] modeled bubble coalescence by considering bubble collisions due to turbulence, buoyancy, and laminar shear and by analysis of the coalescence efficiency of collisions. It was assumed that collisions from these various mechanisms are cumulative, i.e.

$$c(d_i,d_j) = [\varpi_T(d_i,d_j) + \varpi_B(d_i,d_j) + \varpi_{LS}(d_i,d_j)]P_c(d_i,d_j) \quad (7)$$

Turbulent Collision Rate. Prince and Blanch[9] calculated the bubble collision rate by analogy with the gas kinetic theory and assumed that the bubble has the same turbulent velocity of an eddy of the same size. This assumption is reasonable because very small eddies do not contain sufficient energy to significantly affect bubble motion, while eddies much larger than the bubble size transport groups of the bubbles without leading to significant relative motion. The flow was assumed to be isotropic at the length scale of the bubble diameter, and isotropic turbulence theory was used to calculate the eddy turbulent velocity. The final turbulent specific collision rate is

$$\varpi_T(d_i,d_j) = 0.089\pi\epsilon^{1/3}(d_i+d_j)^2(d_i^{2/3}+d_j^{2/3})^{1/2} \quad (8)$$

Buoyancy-Driven Collision Rate. The buoyancy-driven specific collision rate was calculated following work by Friedlander[24] as

$$\varpi_B(d_i,d_j) = 0.25\pi(d_i+d_j)^2|u_{bi}-u_{bj}| \quad (9)$$

where u_b is the bubble rise velocity and was calculated by

$$u_b = (2.14\sigma/\rho_l d + 0.505gd)^{1/2} \quad (10)$$

Laminar Shear Collision Rate. The functional form of the collision rate due to laminar shear was given as

$$\varpi_{LS}(d_i,d_j) = \frac{1}{6}(d_i+d_j)^3(\overline{du_l}/dR)$$

where $\overline{du_l}/dR$ is the average shear rate and was determined by using the correlation of the liquid velocity profile proposed by Walters and Blanch[25] and the correlation of the centerline liquid circulation velocity by Miyauchi and Shyu.[26]

Coalescence Efficiency. Prince and Blanch[9] used eq 6 to calculate the coalescence efficiency and estimated the coalescence time by modeling the thinning of the liquid film between bubbles. The final expression reads

$$P_c(d_i,d_j)=\exp(-t_{ij}/\tau_{ij}) = \exp\left(-\frac{r_{ij}^{5/6}\rho_l^{1/2}\epsilon^{1/3}}{4\sigma^{1/2}}\ln\frac{h_0}{h_f}\right) \quad (11)$$

where the initial film thickness h_0 and the critical film thickness h_f are 10^{-3} and 10^{-6} m for the gas−water system, respectively. The equivalent radius r_{ij} was calculated as $0.5r_ir_j/(r_i+r_j)$.

3.1.2. Bubble Breakup. Prince and Blanch[9] considered the bubble breakup to be caused by collisions by turbulent eddies of sizes equal to or smaller than the bubble size. They argued that eddies smaller than 0.2 of the bubble size are unlikely to contribute significantly to the overall breakup rate and set the lower limit of the effective turbulent eddies as $0.2d$. They considered only eddies having a velocity larger than the critical velocity, where the disruptive force due to the kinetic energy of the eddy and the cohesive force due to surface tension balance each other. They finally gave the breakup rate in a discrete form. For comparison with other models, an equally continuous form eq 12 was used. Prince's breakup model does not include the

daughter bubble size distribution, and a uniform function was used in this work.

$$b(d) = \int_{0.2d}^{d} \frac{0.07\pi^4}{\lambda^4}(d+\lambda)^2(d^{2/3}+\lambda^{2/3})^{1/2}\epsilon^{1/3} \times \exp\left(-\frac{1.18}{\lambda^{2/3}}\frac{\sigma}{\rho_l d\epsilon^{2/3}}\right) d\lambda \quad (12)$$

3.2. Models of Luo and Svendsen. 3.2.1. Bubble Coalescence. Luo and Svendsen[13] only considered bubble coalescence due to turbulence. Their model is similar to that of Prince and Blanch[9] in the calculation of the bubble collision frequency except using different coefficients. The bubble contact time was calculated based on energy conservation during the bubble collision. The bubble collision frequency and the coalescence efficiency are as follows:

$$\varpi_c(d_i,d_j) = \frac{\pi}{4}\sqrt{2}\epsilon^{1/3}(d_i+d_j)^2(d_i^{2/3}+d_j^{2/3})^{1/2} \quad (13)$$

$$P_c(d_i,d_j) = \exp\left(-\frac{t_{ij}}{\tau_{ij}}\right) = \exp\left\{-c_e\frac{[0.75(1+\xi_{ij}^{2})(1+\xi_{ij}^{3})]^{1/2}}{(\rho_g/\rho_l+\gamma)(1+\xi_{ij})^3}We_{ij}^{1/2}\right\} \quad (14)$$

where $\xi_{ij} = d_i/d_j$, γ is the virtual mass coefficient and is set as 0.5 in this work, We_{ij} is the Weber number defined as $\rho_l d_i \hat{u}_{ij}/\sigma$ with $\hat{u}_{ij} = (\hat{u}_i^2 + \hat{u}_j^2)^{1/2}$, and c_e is a model parameter of order unity. c_e was set as 1.0 unless otherwise specified in this work. Luo[27] suggested that $c_e = 0.4$ for the heterogeneous flow regime; therefore, the influence of c_e was also studied in this work, and the results show that the change from $c_e = 1.0$ to 0.4 does not lead to a remarkable influence on the calculated bubble size distribution.

3.2.2. Bubble Breakup. Luo and Svendsen[14] proposed a bubble breakup model based on the theories of isotropic turbulence and probability. This model gave the bubble breakup rate and the daughter size distribution simultaneously and has therefore been widely used in recent years. The bubble breakup rate $b(d)$ and the daughter bubble size distribution $\beta(f_v,d)$ of this model are

$$b(d) = \int_0^{0.5} b(f_v|d)\, df_v \quad (15)$$

$$\beta(f_v,d) = \frac{2b(f_v|d)}{\int_0^1 b(f_v|d)df_v} \quad (16)$$

where $b(f_v|d)$ is calculated as

$$b(f_v|d) = 0.923(1-\alpha_g)n\left(\frac{\epsilon}{d^2}\right)^{1/3}\int_{\xi_{min}}^{1}\frac{(1+\xi)^2}{\xi^{11/3}} \times \exp\left(-\frac{12c_f\sigma}{\beta\rho_l\epsilon^{2/3}d^{5/3}\xi^{11/3}}\right) d\xi \quad (17)$$

3.3. Models of Lehr et al. 3.3.1. Bubble Coalescence. Lehr et al.[17] considered bubble coalescence due to turbulence and due to different rise velocities and calculated the total breakup rate as

$$c(d_i,d_j) = \frac{\pi}{4}(d_i+d_j)^2\min(u',u_{crit})\exp\left[-\left(\frac{\alpha_{g,max}^{1/3}}{\alpha_g^{1/3}}-1\right)^2\right] \quad (18)$$

$$u' = \max(\sqrt{2}\epsilon^{1/3}\sqrt{d_i^{2/3}+d_i^{2/3}}, |u_i-u_j|) \quad (19)$$

where u_{crit} is a model parameter and has the value of 0.08 m/s for the air−water system and $\alpha_{g,max}$ is the maximum possible gas fraction and was set as 0.6.

3.3.2. Bubble Breakup. Lehr et al.[17] modeled bubble breakup followed by the approach of Luo and Svendsen.[14] The difference is that they used the capillary constraint and assumed that the interfacial force and the inertial force balance each other. The formulations of $b(d)$ and $\beta(f_v,d)$ in terms of $b(f_v|d)$ are the same as eqs 15 and 16, and $b(f_v|d)$ is as follows:

$$b(f_v|d) = \int_{d_1}^{d} 0.8413\sqrt{2} \times \frac{\sigma}{\rho_l\epsilon^{2/3}d_1^{4}}\frac{(\lambda+d)^2}{\lambda^{13/3}}\exp\left(-\frac{2\sigma}{\rho_l\epsilon^{2/3}d_1\lambda^{2/3}}\right) d\lambda \quad (20)$$

where d_1 is the diameter of the smaller daughter bubble.

3.4. Models of Wang et al. 3.4.1. Bubble Coalescence. Wang et al.[23] considered three bubble coalescence mechanisms, namely, coalescence due to turbulent eddies, coalescence due to wake entrainment, and coalescence due to different rise velocities. The total bubble coalescence rate is the sum of the coalescence rates due to these three mechanisms, i.e.

$$c(d_i,d_j) = \varpi_T P_T + \varpi_W P_W + \varpi_U P_U \quad (21)$$

Coalescence due to Turbulent Eddies. Wang et al.[23] took into account the influence of the gas fraction on the bubble collision frequency due to turbulent eddies, and the final expression of ϖ_T reads

$$\varpi_T(d_i,d_j) = \frac{\pi}{4}\frac{\alpha_{g,max}}{\alpha_{g,max}-\alpha_g}\Gamma_{ij}\sqrt{2}\epsilon^{1/3}(d_i+d_j)^2(d_i^{2/3}+d_j^{2/3})^{1/2} \quad (22)$$

Compared with Prince's and Luo's models, eq 22 includes modifications for two effects: $\alpha_{g,max}/(\alpha_{g,max}-\alpha_g)$ accounts for the influence of the reduction of the free space for bubble movement due to the volume occupied by bubbles, following work by Hibiki and Ishii,[28] but a value of 0.8 was used for $\alpha_{g,max}$ with the consideration that the value of $\alpha_{g,max}$ in a gas−liquid flow can be larger than that corresponding to the limit of equal closed packed bubbles due to the bubble size distribution; Γ_{ij} accounts for the influence of the ratio between the bubble separation distance and the bubble turbulent path length and is calculated as

$$\Gamma_{ij} = \exp[-(h_{b,ij}/l_{bt,ij})^6] \quad (23)$$

where $l_{bt,ij}$ is the mean relative turbulent path length of bubbles of size d_i and d_j:

$$l_{bt,ij} = (l_{bt,i}^{2} + l_{bt,j}^{2})^{1/2} \quad (24)$$

The bubble turbulent path length l_{bt} was assumed to be equal to the distance that a turbulent eddy of size d_b moves during its lifetime τ_e:

$$l_{bt} = \bar{u}_{bt}\tau_e \approx 0.89 d_b \tag{25}$$

$h_{b,ij}$ in eq 23 is related to the mean distance between bubbles of size d_i and d_j:

$$h_{b,ij} = k(n_i + n_j)^{-1/3} \tag{26}$$

where $n_i = N_i/\Delta d_i$ and k was set as 6.3.

Equation 14 was used to calculate the bubble coalescence efficiency with the same parameter settings.

Coalescence due to Wake Entrainment. A large bubble with sphere-cap shape has a strong wake region. Other bubbles will be accelerated when entering such bubble wake regions, resulting in bubble collision and coalescence. Wang et al.[23] extended the model for coalescence due to wake entrainment for the two-group case proposed by Hibiki and Ishii[28] to the multigroup case. It was assumed that only bubbles larger than d_c have a wake region effective for bubble coalescence. The formulations are as follows:

$$c_W(d_i,d_j) = 15.4\Theta d_i^{\,2}\bar{u}_{slip,i}\exp\{-0.46\rho_l^{1/2}\epsilon^{1/3}\sigma^{-1/2}[d_i d_j/(d_i + d_j)]^{5/6}\} \tag{27}$$

$$\bar{u}_{slip,i} = 0.71\sqrt{g d_i} \tag{28}$$

$$\Theta = \begin{cases} (d_j - d_c/2)^6/[(d_j - d_c/2)^6 + (d_c/2)^6] & d_j \geq d_c/2 \\ 0 & \text{else} \end{cases} \tag{29}$$

$$d_c = 4\sqrt{\sigma/g\Delta\rho} \tag{30}$$

Coalescence due to Different Rise Velocities. The model for the bubble collision frequency due to different rise velocities is similar to that due to turbulent eddies, except the characteristic velocity $(\hat{u}_i^2 + \hat{u}_j^2)^{1/2}$ is replaced by the relative rise velocity, which is assumed to be equal to $|u_{ri} - u_{rj}|$. The rise velocity of bubbles in the ith group, u_{ri}, is calculated using the Fan−Tsuchiya equation.[29] Because the bubbles rise vertically, the modification by eq 23 is unnecessary. With the consideration that the coalescence efficiency for collision due to different rise velocities may be different from that due to turbulence, the bubble coalescence efficiency was set as 0.5 by fitting the experimental data at low gas fractions.

3.4.2. Bubble Breakup. Two mechanisms are considered for bubble breakup, namely, breakup due to turbulent eddies and due to the instability of large bubbles.

Breakup due to Turbulent Eddies. Wang et al.[18] proposed a breakup kernel function based on the eddy−bubble interaction mechanism followed by Luo and Svendsen.[14] This model took into account both the energy constraint and capillary force constraint. The formulations of $b(d)$ and $\beta(f_v,d)$ in terms of $b(f_v|d)$ are the same as eqs 15 and 16, and $b(f_v|d)$ is determined by the following equations:

$$b(f_v|d) = 0.923(1 - \alpha_g)\epsilon^{1/3}\int_{\lambda_{min}}^{d} P_b(f_v|d,\lambda) \times (\lambda + d)^2\lambda^{-11/3}\,d\lambda \tag{31}$$

$$P_b(f_v|d,\lambda) = \int_0^\infty P_b[f_v|d,e(\lambda),\lambda]\,P_e[e(\lambda)]\,de(\lambda) \tag{32}$$

$$P_e[e(\lambda)] = [1/\bar{e}(\lambda)]\exp[-e(\lambda)/\bar{e}(\lambda)] \tag{33}$$

$$\bar{e}(\lambda) = (1/12)\pi\lambda^3\rho_c\bar{u}_\lambda^{\,2} \tag{34}$$

$$P_b[f_v|d,e(\lambda),\lambda] = \begin{cases} (f_{v,max} - f_{v,min})^{-1} & f_{v,max} - f_{v,min} \geq \delta \text{ and } f_{v,min} < f_v < f_{v,max} \\ 0 & \text{else} \end{cases} \tag{35}$$

$$c_{f,max} = \min[(2^{1/3}-1), e(\lambda)/\pi d^2\sigma] \tag{36}$$

$$f_{v,min} = \{\pi\lambda^3\sigma/[6e(\lambda)\,d]\}^3 \tag{37}$$

where λ_{min} is the minimum size of eddies effective for bubble breakup. The details can be found in our previous work.[18,30]

Breakup due to Instability. A bubble with size larger than a certain critical value will break up quickly because of the instability of the interphase. The following empirical equation was used to calculate the bubble breakup rate due to instability:

$$b_2(d) = b^* \frac{(d - d_{c2})^m}{(d - d_{c2})^m + d_{c2}^{\,m}} \tag{38}$$

where d_{c2} is the critical bubble diameter set as 27 mm as followed by Carrica and Clausse.[31] b^* and m are model parameters and were set as 100 1/s and 6.0, respectively. Because detailed studies are not available for this bubble breakup process, the bubble was assumed to break into two equal daughter bubbles considering that the nonuniform breakup of a large bubble was already included in the breakup model due to turbulence mechanism. In fact, the bubble size distribution is not sensitive to the breakup due to instability.[23]

4. Results and Discussion

4.1. Bubble Breakup Rate. Parts a and b of Figure 1 show the bubble breakup rates due to turbulence predicted by different models when the energy dissipation rate is 0.2 and 1.0 m^2/s^3, respectively. Lehr et al.[17] compared the bubble breakup rate calculated by their model with the experimental data of Martíez-Bazán et al.[15] and obtained a good agreement. The bubble breakup rates by Wang's model are quite close to those by Lehr's model except Wang's model predicts a higher breakup rate in the small bubble range. Note that in Wang's model the value of the parameter δ in eq 35 has influence on the bubble breakup rate for large bubbles and large energy dissipation rates. When δ is set as 0.0001, the bubble breakup rates by Wang's model are close to those by Lehr's model for bubble sizes up to 20 mm; when δ is set as 0.01, the bubble breakup rates by Wang's model are slightly smaller than those by Lehr's model at large energy dissipation rates. Further calculations show that the value of δ has no significant influence on the bubble size distribution when $\delta < 0.01$. This is because a large bubble mainly breaks into a very small bubble and a large complement bubble due to the turbulence mechanism at large dissipation rates, as shown in Figure 2c. In such cases, some decrease in the bubble breakup rate does not result in a remarkable variation in the bubble size. Prince's model gives a much higher bubble breakup rate, while Luo's model gives

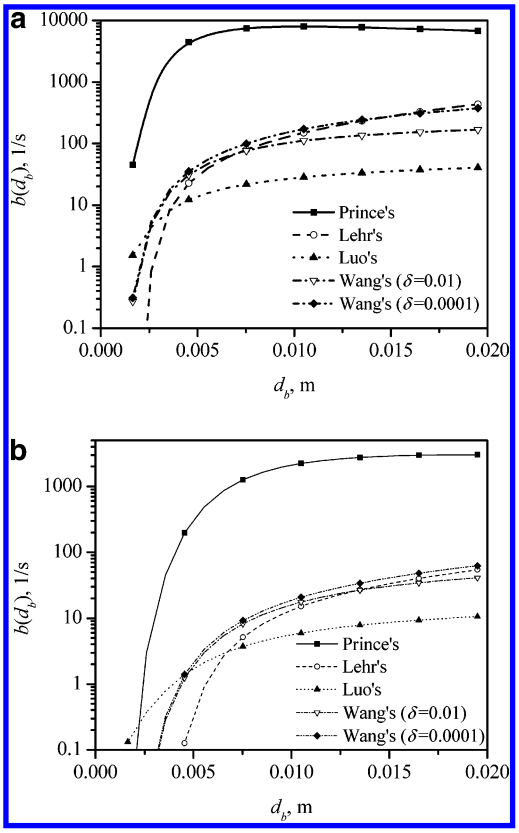

Figure 1. Bubble breakup rate calculated by different models: (a) air−water system with $\epsilon_l = 1.0$ m^2/s^3; (b) air−water system with $\epsilon_l = 0.2$ m^2/s^3.

lower predictions. In terms of the bubble breakup rate, both Lehr's and Wang's models give reasonable results.

The main difference of the above bubble breakup models lies in the formulation of the breakup efficiency. Prince's model simply correlates the bubble breakup efficiency to the ratio between the mean turbulent velocity of eddies and a critical velocity. This leads to a value close to 1.0 of the breakup efficiency in most cases, and therefore the bubble breakup rate is overpredicted. Luo's model only considers the energy constraint and ignores the capillary constraint during the bubble breakup; that is, breakup occurs only if the kinetic energy of an eddy is larger than the increase of the surface energy due to bubble breakup. Other unreasonable aspects of Luo's model were discussed in work by Wang et al.[18] Lehr's model only considers the capillary constraint and assumes that the interfacial force and the inertial force balance each other. Wang's model considers both the energy constraint and capillary constraint.

4.2. Daughter Bubble Size Distribution. From experiments and models available in the literature and the analysis of the bubble breakup process, we have concluded that a daughter bubble size distribution should have the following characteristics:[18] (1) a local minimum probability exists at exactly equal breakup; (2) the daughter bubble size distribution depends on the mother bubble size and the energy dissipation rate; (3) the daughter bubble size distribution function should vanish when the breakup fraction f_v approaches zero; (4) the daughter bubble size distribution should have no singularity point.

Parts a−c of Figure 2 compare the daughter bubble size distributions of different bubble breakup models. Prince and Blanch[9] used a uniform daughter bubble size

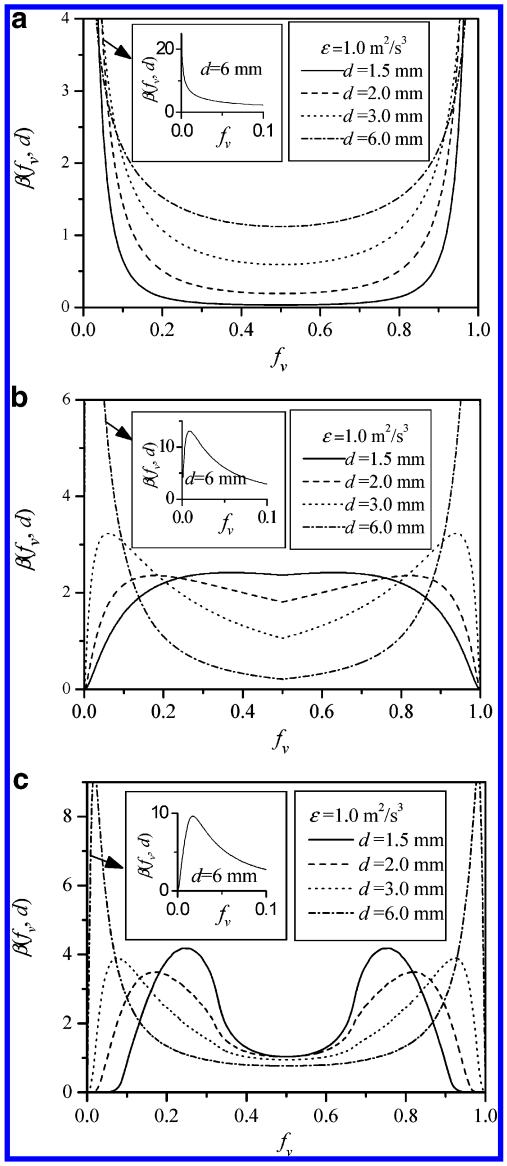

Figure 2. Daughter bubble size distribution: (a) by Luo's model (air−water system); (b) by Lehr's model (air−water system); (c) by Wang's model (air−water system).

distribution, and their result is not shown in the figures. Luo's model predicts a U-shaped daughter bubble size distribution, only satisfies characteristics 1, 2, and 4, and predicts a too high fraction of small bubbles because the capillary constraint is ignored. Both Lehr's and Wang's models predict an M-shaped daughter bubble size distribution. Lehr's model satisfies characteristics 1−3, but does not satisfy characteristic 4 with a singularity point at $f_v = 0.5$ that may be caused by their assumption that the interfacial force of the bubble surface and the inertial force of the colliding eddy balance each other. Wang's model considers both the energy constraint and capillary constraint, and the predicted daughter bubble size distributions satisfy all of the characteristics mentioned above. Both Lehr's and Wang's models predict a more nonuniform breakup for larger bubbles and larger dissipation rates, while Luo's model predicts a contrary tendency. For a small bubble, nonuniform breakup means that a very small bubble and a complement bubble will be generated. This probability is highly small because the generation of a very small bubble is limited by the capillary constraint. Therefore, Lehr's and Wang's models properly describe

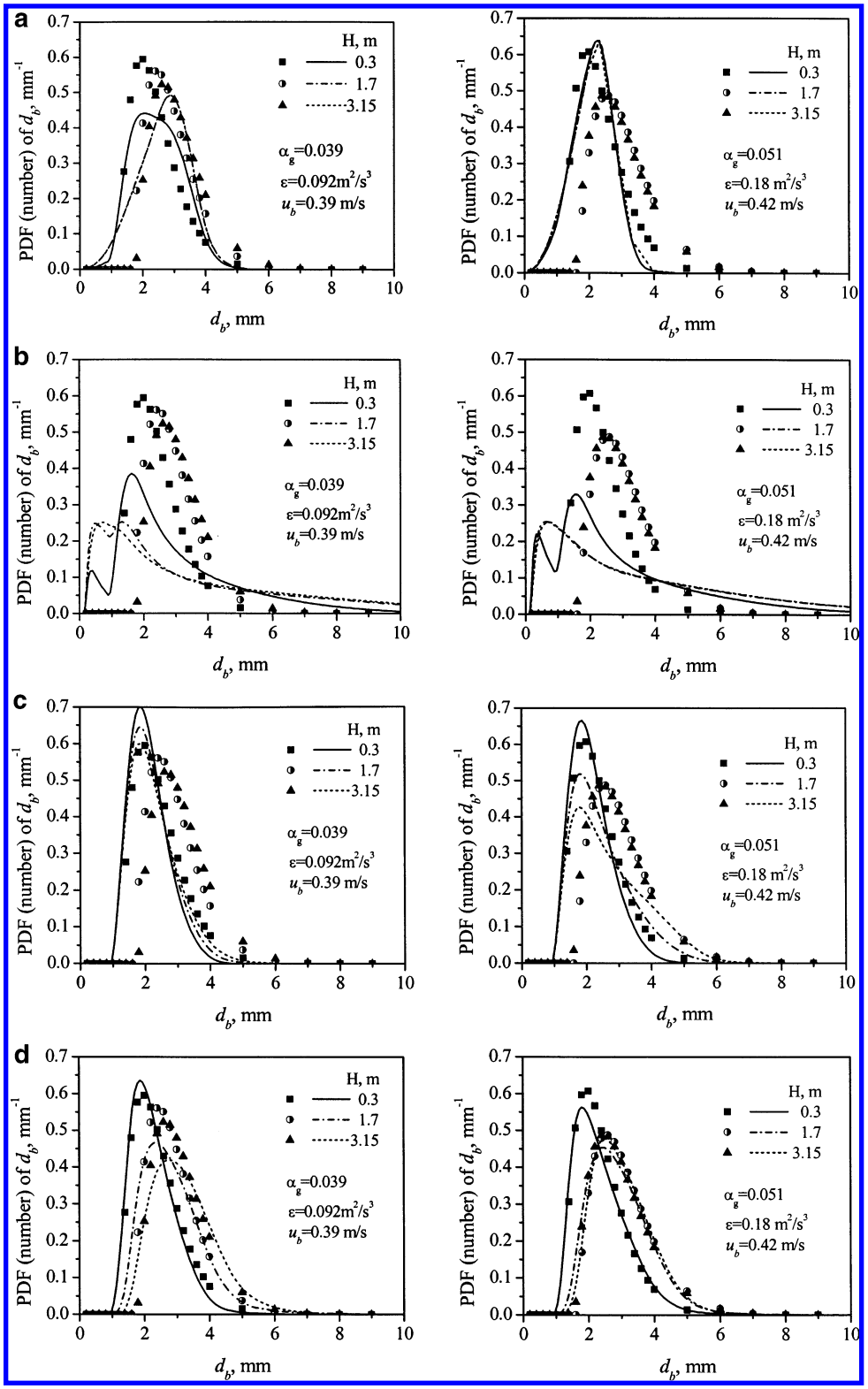

Figure 3. (a) Axial evolution of the bubble size distribution (air−water system, column i.d. is 0.23 m; left, $U_g = 0.016$ m/s, $U_l = 0.17$ m/s; right, $U_g = 0.024$ m/s, $U_l = 0.19$ m/s). Measurements (symbols: our results) vs predictions (lines) by Prince's model. (b) Axial evolution of the bubble size distribution (conditions are the same as those in part a). Measurements (symbols: our results) vs predictions (lines) by Luo's model. (c) Axial evolution of the bubble size distribution (conditions are the same as those in part a). Measurements (symbols: our results) vs predictions (lines) by Lehr's model. (d) Axial evolution of the bubble size distribution (conditions are the same as those in part a). Measurements (symbols: our results) vs predictions by Wang's model.

the influences of the bubble size and energy dissipation rate on the daughter bubble size distribution.

4.3. Bubble Size Distribution. The steady-state version of eq 2 was solved to give the bubble size distribution with the bubble breakup and coalescence models given above. In all calculations in this work, constant values of α_g, ϵ, and u_b from either measurements, correlations, or CFD simulations were used. At medium-to-high gas fractions, the equilibrium bubble size distribution is approached quickly and only the equilibrium bubble size distributions are shown in such conditions. Two bubble size distributions are used: one

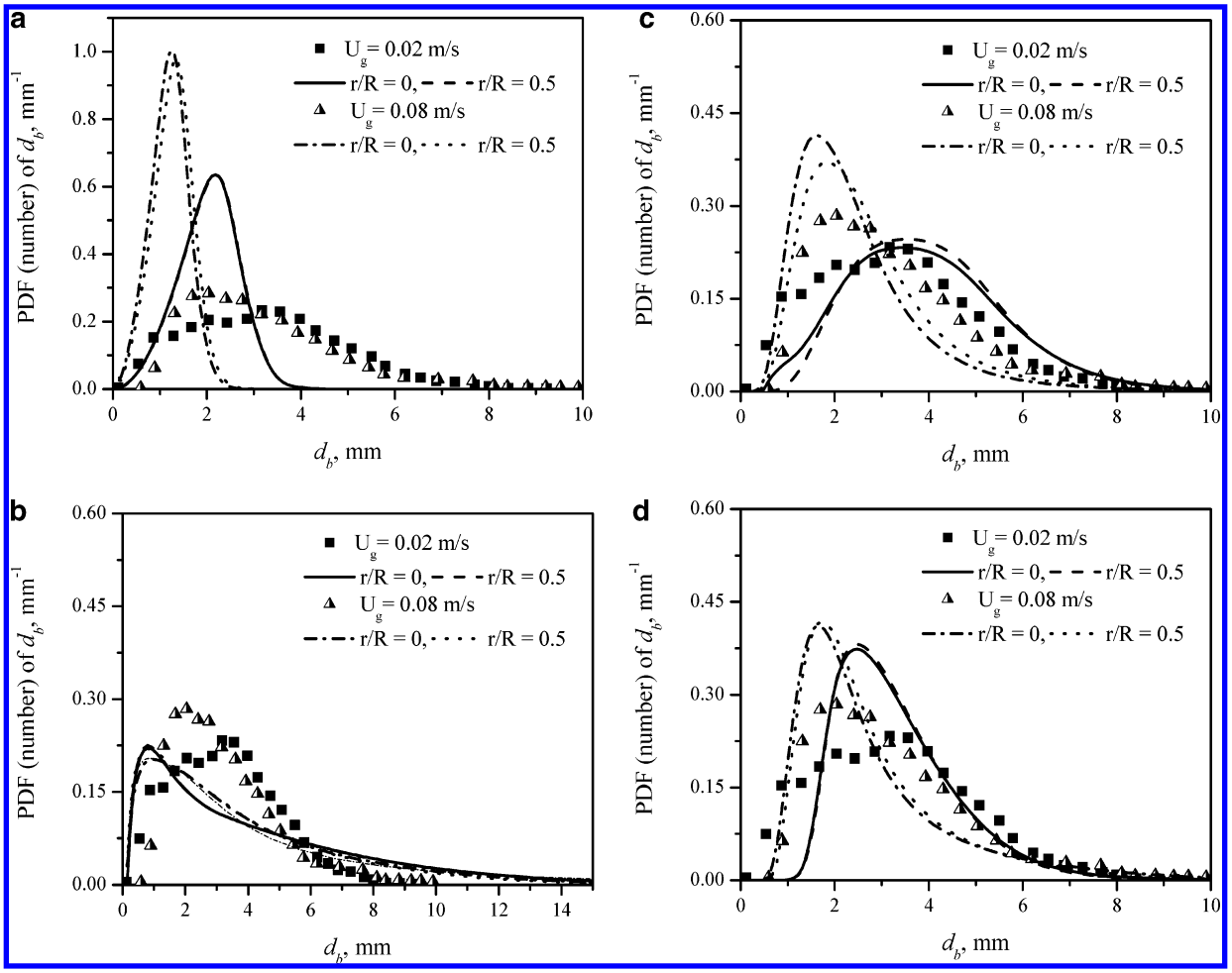

Figure 4. Bubble size distribution at different gas fractions and dissipation rates (air−water system). (a) Measurements (symbols: from Lehr et al.[17]) vs predictions (lines) by Prince's model. $U_g = 0.02$ m/s: $\alpha_g = 0.095$ and $\epsilon_l = 0.232$ m^2/s^3 for $r/R = 0$; $\alpha_g = 0.089$ and $\epsilon_l = 0.225$ m^2/s^2 for $r/R = 0.5$. $U_g = 0.08$ m/s: $\alpha_g = 0.33$ and $\epsilon_l = 1.35$ m^2/s^3 for $r/R = 0$; $\alpha_g = 0.22$ and $\epsilon_l = 0.981$ m^2/s^3 for $r/R = 0.5$. (b) Measurements (symbols: from Lehr et al.[17]) vs predictions (lines) by Luo's model. Solid line: $c_e = 1.0$. Dotted line: $c_e = 0.4$. $U_g = 0.08$ m/s, and $r/R = 0$. Values of α_g and ϵ_l are the same as those in part a. (c) Measurements (symbols: from Lehr et al.[17]) vs predictions (lines) by Lehr's model. Values of α_g and ϵ_l are the same as those in part a. (d) Measurements (symbols: from Lehr et al.[17]) vs predictions by Wang's model. Values of α_g and ϵ_l are the same as those in part a.

is $PDF_n(d_b)$, expressed as the number probability density function (PDF) with respect to the bubble diameter; the other is $PDF_f(d_b)$, expressed as the volume fraction PDF with respect to the bubble diameter. $PDF_n(d_b)$ and $PDF_f(d_b)$ are correlated to the bubble number density $n(v)$ by

$$PDF_n(d_b) = n(v)\, {d_b}^2 / \int_0^\infty n(v)\, {d_b}^2\, \mathrm{d}d_b \qquad (39)$$

$$PDF_f(d_b) = n(v)\, {d_b}^5 / \int_0^\infty n(v)\, {d_b}^5\, \mathrm{d}d_b \qquad (40)$$

The bubble size was divided into 30 sections using a geometric grid with $v_{i+1}/v_i = 1.7$ and $v_1 = 10^{-10}$ m^3 for calculation of $PDF_f(d_b)$ and $v_{i+1}/v_i = 1.45$ and $v_1 = 10^{-12}$ m^3 for $PDF_n(d_b)$.

The CFD model used in this work was similar to that in Wang et al.[32] except for the different treatments of the drag force and turbulence modification. To describe the different phase interactions in the heterogeneous and homogeneous regimes, the drag model of Krishna et al.[33] was used to calculate the average bubble rise velocity, which, in turn, was used to calculate the drag coefficient. The two-time-constant turbulence modeling modification proposed by Lopez de Bertodano et al.[34] was used to modify the influence of the bubbles on liquid turbulence. The model was validated with the experimental results, and the details can be found in our previous work.[23,32]

4.3.1. Low Gas Fraction. At low gas fractions, bubble breakup is weak and bubble coalescence determines the evolution of the bubble size distribution. We measured the axial evolution of the bubble size distribution in an external-loop airlift reactor with a fiber-optic probe. The typical results at low gas fractions are shown in Figure 3. The detailed description of the measurement technique can be found elsewhere.[35] Because of bubble coalescence, the bubbles become larger along the axial height. The evolution of the bubble size distribution to equilibrium is faster at a gas fraction of 0.051 than at a gas fraction of 0.039.

Parts a−d of Figure 3 compare the PBM predictions with different bubble coalescence and breakup models. The measured average values at the centerline for the gas holdup and bubble rise velocity were used in the calculation. The dissipation rate was calculated from the CFD simulation using a single bubble class with an average size. The bubble size distribution measured near the gas distributor was used as the inlet boundary condition for the PBM. The bubble size distributions predicted by Prince's model have a much smaller mean value than the experimental results and approach the

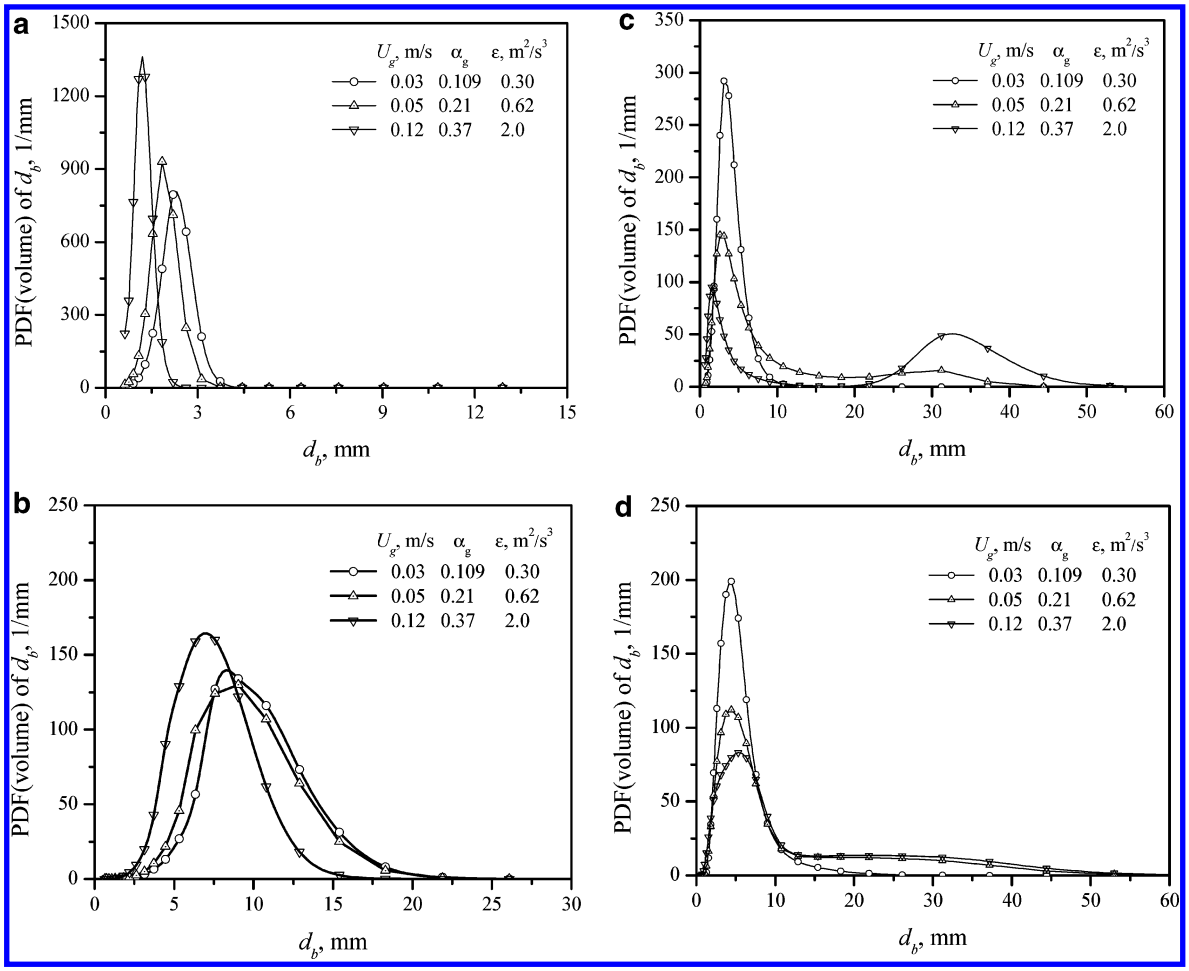

Figure 5. Bubble size distribution in the centerline of the column in different flow regimes (air−water system, i.d. = 0.19 m, H = 2.5 m): (a) predicted by Prince's model; (b) predicted by Luo's model; (c) predicted by Lehr's model; (d) predicted by Wang's model.

equilibrium distribution too fast. This is caused by the high bubble breakup rate and by the fact that the influence of the gas fraction on the coalescence rate in their models is ignored. Luo's model overpredicts the fractions of both large bubbles and very small bubbles. The overprediction of large bubbles is due to the fact that the influence of the gas fraction on the bubble coalescence rate is ignored, and the overprediction of very small bubbles is due to the unreasonably high fraction of very small bubbles in the daughter bubble size distribution. Lehr's model underpredicts the increase in the bubble size at a gas fraction of 0.039. In Lehr's model, modifications accounting for the influence of the gas fraction were made to coalescence rates due to both turbulent eddies and different rise velocities. The influence of the gas fraction is related to the ratio between the bubble turbulent path length and the distance between bubbles. When the gas fraction is low, the distance between bubbles becomes larger than the bubble turbulent path length. This will cause a decrease in the bubble collision rate due to turbulence. For bubble collision due to different rise velocities, the gas fraction has no such influence because all bubbles generally rise vertically. Therefore, Lehr's model underpredicts the bubble coalescence rate due to different rise velocities at low gas fractions. At a gas fraction of 0.051, Lehr's model does not predict the tendency that the bubble size distribution approaches equilibrium along the axial height. This is related to the underprediction of the breakup rate for small bubbles and the overprediction of the bubble coalescence rate due to different rise velocities at low gas fractions. Thus, the bubble breakup and coalescence do not approach equilibrium within the axial range in Figure 3. Wang's model gives reasonable results for the evolution of the bubble size distribution. The bubble coalescence at low gas fractions in Wang's model is mainly due to different rise velocities. The bubble rise velocity decreases fast when the bubble size is smaller than 2 mm; therefore, the coalescence rate of small bubbles is relatively large, and the number of small bubbles remarkably decreases along the axial height. Figure 3d shows that the tendency of approaching an equilibrium bubble size distribution is also predicted.

4.3.2. Medium-to-High Gas Fraction. Parts a−d of Figure 4 compare the predictions by the PBM with the experimental data from Lehr et al.[17] at medium-to-high gas fractions when different bubble coalescence and breakup models are used. Because the radial profiles of the turbulence dissipation rate and gas holdup are nonuniform at medium-to-high gas fractions, the results from CFD simulations were used in the calculations of PBM. The simulated column is 2.5 m in height and 0.19 m in inner diameter. Note that the radial position of the measured bubble size distribution was not specified in work by Lehr et al.;[17] the calculated bubble size distributions for r/R = 0 and 0.5 are compared with the experimental results. Prince's model properly predicts the variation of the peak poison of the bubble size distribution with the gas fraction, but the predicted mean bubble size is much smaller than the measured value. Furthermore, the shape of the predicted bubble

size distribution is close to a normal distribution, while the measured bubble size distribution is approximately log normal. Luo's model overpredicts the fractions of both large bubbles and small bubbles and underpredicts the variation of the bubble size distribution with the gas faction. Both Lehr's and Wang's models give reasonable predictions at gas fractions of 0.08 and 0.20. Because of the limitation of probe techniques for bubble measurement, the experimental results usually have a larger uncertainty for very small bubbles due to surface tension and for large bubbles due to bubble deformation. This is a reason that the discrepancies in parts c and d of Figure 4 are somewhat large. Note that the results shown in Figure 4c for a gas fraction of 0.08 are a little bit different from that reported by Lehr et al.[17] The results in Figure 4c are the equilibrium bubble size distributions, and the results in work by Lehr et al.[17] may be the bubble size distributions before the equilibrium is approached.

4.4. Regime Transition. The hydrodynamics in a bubble column are characterized by different flow regimes, i.e., the homogeneous and heterogeneous regimes, depending on the superficial gas velocity. The homogeneous regime occurs at low superficial gas velocities and turns into the heterogeneous regime with an increase in the superficial gas velocity. The homogeneous regime is characterized in a uniform radial profile of the gas fraction and a narrow bubble size distribution. With an increase in the superficial gas velocity and gas fraction, the radial profile of the gas fraction becomes nonuniform and bubble coalescence and breakup become stronger, which leads to a wide bubble size distribution and an increase in the volume fraction of large bubbles. If the bubble size distributions at different gas velocities are correctly predicted, then the flow regime transition can be distinguished based on the variation of the bubble size distribution.

Parts a−d of Figure 5 compare the predicted bubble size distributions at the centerline in a bubble column in different flow regimes when different bubble coalescence and breakup models are used. The gas fraction and energy dissipation rate are from CFD simulations on a bubble column of 2.5 m in height and 0.19 m in inner diameter. The CFD and PBM are, in principle, coupled to each other. For simplification, the CFD model in this work does not calculate the interphase forces and turbulence modification based on the bubble size distribution from the PBM but uses the two bubble class models of Krishna et al.[33] The calculated flow field was then used to calculate the PBM. Both Prince's and Luo's models fail to predict the formation of large bubbles in the heterogeneous regime and predict a tendency that bubbles become smaller with increasing superficial gas velocity, which is contrary to the experimental observation. Both Lehr's and Wang's models successfully predict the remarkably different bubble size distributions in different flow regimes and the formation of large bubbles in the heterogeneous regime. The results by Lehr's and Wang's models are quite similar at superficial gas velocities of 0.03 and 0.05 m/s. At the superficial gas velocity of 0.012 m/s, Lehr's model predicts a distinct bimodal bubble size distribution with two peaks at about 2.0 and 32 mm, respectively. The volume fractions of bubbles between 10 and 20 mm are almost zero, which seems unreasonable from both experimental observation and theoretical analysis.

5. Conclusions

In this work, several bubble coalescence and breakup models were compared. The results show that the bubble size distributions predicted by the PBM are quite different when different bubble breakup and coalescence models are used. By using appropriate bubble breakup and coalescence models, the bubble size distribution and regime transition can be reasonably predicted. Among the models compared in this work, Prince's and Luo's models do not give good predictions of the bubble size distribution, but these models provided the basic concepts for modeling bubble coalescence and breakup, which were widely used by other researchers to propose improved models. Lehr's model gives reasonable results at medium-to-high gas velocities, except they predict a too distinct bimodal distribution with nearly zero fractions of bubbles between 10 and 20 mm. In Lehr's model, modification accounting for the influence of the gas fraction was also made to bubble coalescence due to different rise velocities, leading to a poor prediction of the bubble size distribution at low gas fraction. Wang's model generally gives reasonable results for all of the conditions studied in this work. From the results, we can also draw the following conclusions: (1) The M-shaped daughter bubble size distribution as predicted by Lehr's and Wang's models is reasonable. (2) It is necessary to take into account bubble coalescence and breakup due to different mechanisms. (3) The modification accounting for the influence of the gas fraction on bubble coalescence due to turbulence should be considered, while such a modification is unnecessary for bubble coalescence due to different rise velocities and wake entrainment.

Acknowledgment

The authors gratefully acknowledge financial support by the National Science Foundation of China (Grant 20276035).

Notations

$b(d)$ = specific bubble breakup rate due to turbulent eddies, 1/s
$b_2(d)$ = specific bubble breakup rate due to bubble instability, 1/s
$b(f_v|d)$ = breakup rate of a bubble of size d breaking with breakup fraction f_v, 1/s
$c(d_i,d_j)$ = bubble coalescence rate, m^3/s
d = bubble diameter, m
d_c = critical bubble diameter effective for wake-induced coalescence, m
d_{c2} = critical bubble diameter effective for breakup due to instability, m
f_v = breakup fraction
g = bubble size pivot, m^3
h_b = distance between bubbles, m
l_{bt} = bubble turbulent path length, m
L_w = effective bubble wake length, m
$n(v)$ = number density of the bubbles, $1/m^6$
N_i = bubble number in the ith bubble subregion per volume, $1/m^3$
$P(d_i,d_j)$ = coalescence efficiency
$P_b(f_v|d,\lambda)$ = breakup probability density for a bubble of size d breaking with breakup fraction f_v when hit by an eddy of size λ
$PDF_n(d_b)$ = number probability density function with respect to the bubble diameter, 1/m

$PDF_f(d_b)$ = volume fraction probability density function with respect to the bubble diameter, 1/m
$t_{i,j}$ = bubble contact time, s
$\hat{u}_\lambda$ = mean turbulent velocity of an eddy, m/s
$\hat{u}_{b,slip}$ = bubble slip velocity, m/s
$\hat{u}_{bt}$ = mean turbulent velocity of a bubble, m/s
U_g = superficial gas velocity, m/s
U_l = superficial liquid velocity, m/s
v = volume of the mother bubble, m^3
We = Weber number, $\rho d u^2/\sigma$

Greek Letters

α = phase fraction
$\beta(f_v,d)$ = daughter bubble size distribution
γ = coefficient of virtual mass
ρ = density, kg/m^3
λ = eddy size, m
ϵ = energy dissipation rate, m^2/s^3
λ_{min} = minimum eddy size effective for breakup, m
$\varpi(d_i,d_j)$ = bubble collison frequency, m^3/s
$\tau_{i,j}$ = time required for coalescence, s
τ_e = lifetime of a turbulent eddy, s
$\Gamma_{i,j}$ = coefficent related to the bubble distance
$\eta_{i,j,k}$ = distributing coefficient related to bubble coalescence
$\zeta_{i,k}$ = distributing coefficient related to bubble breakup
$\xi_{i,j}$ = relative size defined as d_i/d_j
Θ = coefficent related to the critial bubble size d_c

Subscripts

b = bubble
g = gas phase
l = liquid phase

Literature Cited

(1) Hulburt, H.; Katz, S. Some Problems in Particle Technology: a Statistical Mechanical Formulation. *Chem. Eng. Sci.* **1964**, *19*, 555.

(2) Ramkrishna, D.; Mahoney, A. W. Population Balance Modeling. Promise for the Future. *Chem. Eng. Sci.* **2002**, *57*, 595.

(3) Kostoglou, M.; Karabelas, A. J. On the Attainment of Steady State in Turbulent Pipe Flow of Dilute Dispersions. *Chem. Eng. Sci.* **1998**, *53*, 505.

(4) Millies, M.; Mewes, D. Interfacial Area Density in Bubble Flow. *Chem. Eng. Process.* **1999**, *38*, 307.

(5) Colella, D.; Vinci, D.; Bagatin, R.; Masi, M.; Bakr, E. A. A Study on Coalescence and Breakage Mechanisms in Three Different Bubble Columns. *Chem. Eng. Sci.* **1999**, *54*, 4767.

(6) Lehr, F.; Mewes, D. A Transport Equation for the Interfacial Area Density Applied to Bubble Columns. *Chem. Eng. Sci.* **2001**, *56*, 1159.

(7) Pohorecki, R.; Moniuk, W.; Bielski, P.; Zdrójkowski, A. Modeling of the Coalescence/Redispersion Processes in Bubble Columns. *Chem. Eng. Sci.* **2001**, *56*, 6157.

(8) Lee, C. H.; Erickson, L. E.; Glasgow, L. A. Bubble Breakup and Coalescence in Turbulent Gas−Liquid Dispersions. *Chem. Eng. Commun.* **1987**, *59*, 65.

(9) Prince, M. J.; Blanch, H. W. Bubble Coalescence and Breakup in Air-Sparged Bubble Columns. *AIChE J.* **1990**, *36*, 1485.

(10) Hesketh, R. P.; Etchells, A. W. Bubble Breakup in Pipeline Flow. *Chem. Eng. Sci.* **1991**, *46*, 1.

(11) Nambiar, D. K. R.; Kumar, R.; Das, T. R.; Gandhi, K. S. A New Model for the Breakup Frequency of Drops in Turbulent Stirred Dispersions. *Chem. Eng. Sci.* **1992**, *47* (12), 2989.

(12) Tsouris, C.; Tavlarides, L. L. Breakage and Coalescence Models for Drops in Turbulent Dispersions. *AIChE J.* **1994**, *40* (3), 395.

(13) Luo, H.; Svendsen, H. F. Modeling and Simulation of Binary Approach by Energy Conservation Analysis. *Chem. Eng. Commun.* **1996**, *145*, 145.

(14) Luo, H.; Svendsen, H. F. Theoretical Model for Drop and Bubble Breakup in Turbulent Dispersions. *AIChE J.* **1996**, *42*, 1225.

(15) Martíez-Bazán, C.; Montañes, J. L.; Lasheras, J. C. On the Break-up of an Air Bubble Injected into a Fully Developed Turbulent Flow. Part I: Break-up Frequency. *J. Fluid Mech.* **1999**, *401*, 157.

(16) Hagesaether, L.; Jakobsen, H. A.; Svendsen, H. F. A Model for Turbulent Binary Breakup of Dispersed Fluid Particles. *Chem. Eng. Sci.* **2002**, *57*, 3251.

(17) Lehr, F.; Millies, M.; Mewes, D. Bubble Size Distributions and Flow Fields in Bubble Columns. *AIChE J.* **2002**, *48* (11), 2426.

(18) Wang, T. F.; Wang, J. F.; Jin, Y. A Novel Theoretical Breakup Kernel Function for Bubbles/Droplets in a Turbulent Flow. *Chem. Eng. Sci.* **2003**, *58*, 4629.

(19) Ramkrishna, D. *Population Balances: Theory and Applications to Particulate Systems in Engineering*; Academic Press: San Diego, CA, 2000.

(20) Kumar, S.; Ramkrishna, D. On the Solution of Population Balance Equation by Discretization−I. A Fixed Pivot Technique. *Chem. Eng. Sci.* **1996**, *51* (8), 1311.

(21) Chesters, A. K. Modeling of Coalescence Processes in Fluid−Liquid Dispersions. A Review of Current Understanding. *Trans. Inst. Chem. Eng.* **1991**, *69* (A), 259.

(22) Fu, X. Y.; Ishii, M. Two-Group Interfacial Area Transport in Vertical Air−Water Flow. I. Mechanistic Model. *Nucl. Eng. Des.* **2002**, *219*, 143.

(23) Wang, T. F.; Wang, J. F.; Jin, Y. Theoretical Prediction of Flow Regime Transition in Bubble Columns by the Population Balance Model. *Chem. Eng. Sci.* **2005**, accepted for publication.

(24) Friedlander, S. K. *Smoke, Dust and Haze*; Wiley: New York, 1977.

(25) Walters, J.; Blanch, H. W. Liquid Circulation Patterns and their Effect on Gas Holdup and Axial Mixing in Bubble Columns. *Chem. Eng. Commun.* **1983**, *19*, 243.

(26) Miyauchi, T.; Shyu, C. N. Fluid Flow in Gas Bubble Columns. *Kagaku Kogaku* **1970**, *34*, 958.

(27) Luo, H. Coalescence, breakup and liquid circulation in bubble column reactors, Ph.D. Thesis, Norwegian Institute of Technology, Trondheim, Norway, 1993.

(28) Hibiki, T.; Ishii, M. Two-Group Interfacial Area Transport Equations at Bubbly-to-Slug Transition. *Nucl. Eng. Des.* **2000**, *202*, 39.

(29) Fan, L. S.; Tsuchiya, K. *Bubble Wake Dynamics in Liquids and Liquid−Solid Suspensions*; Butterworth-Heinemann: Stoneham, MA, 1990.

(30) Wang, T. F.; Wang, J. F.; Jin, Y. An Efficient Numerical Algorithm for "A Novel Theoretical Breakup Kernel Function of Bubble/Droplet in a Turbulent Flow". *Chem. Eng. Sci.* **2004**, *59*, 2593.

(31) Carrica, P. M.; Clausse, A. A. Mathematical Description of the Critical Heat Flux as Nonlinear Dynamic Instability. In *Instabilities in Multiphase Flow*; Gouesbet, G., Berlemont, A., Eds.; Plenum Press: New York, 1993.

(32) Wang, T. F.; Wang, J. F.; Jin, Y. Experimental Study and CFD Simulation of Hydrodynamic Behaviors in an External Loop Airlift Slurry Reactor. *Can. J. Chem. Eng.* **2004**, *82*, 1183.

(33) Krishna, R.; Urseanu, M. I.; van Baten, J. M.; Ellenberger, J. Influence of Scale on the Hydrodynamics of Bubble Columns Operating in the Churn-Turbulent: Experiments vs Eulerian Simulations. *Chem. Eng. Sci.* **1999**, *54*, 4903.

(34) Lopez de Bertodano, M.; Lahey, R. T.; Jones, O. C. Development of a $k-\epsilon$ model for bubbly two phase flow. *J. Fluids Eng.* **1994**, *116* (1), 128.

(35) Wang, T. F.; Wang, J. F.; Yang, W. G.; Jin, Y. Bubble Behavior in Gas−Liquid−Solid Three-Phase Circulating Fluidized Beds. *Chem. Eng. J.* **2001**, *84*, 397.

Received for review November 14, 2004
Revised manuscript received June 9, 2005
Accepted June 14, 2005

IE0489002